

# Hydrophobic Halloysite Nanotubes via Ball Milling for Stable Pickering Emulsions: Implications for Food Preservation

Cuiying Tan, Puxiang Zhao, Youquan Zhou, and Mingxian Liu\*

Cite This: *ACS Appl. Nano Mater.* 2022, 5, 11289–11301

Read Online

ACCESS |



Metrics &amp; More



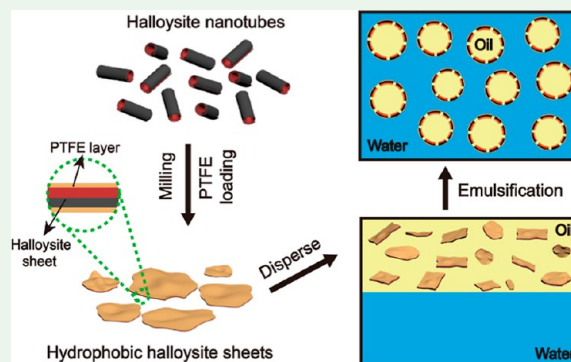
Article Recommendations



Supporting Information

**ABSTRACT:** Modification and functionalization of nanomaterials by a facile way are critical for their practical application in many areas. In this work, hydrophobic modified halloysite nanotubes (mHNTs) were efficiently prepared by a ball milling method; then, the mHNTs were used to stabilize oil/water emulsions. Polytetrafluoroethylene in the wall of milling jars adhered to the surfaces of HNTs during the milling process, which changed the hydrophilicity and electrical properties of HNTs. The milling process reduced the length of the tubes and promoted the transformation of the 1D tubes into 2D sheets morphology. mHNTs were then employed as solid particles on the oil–water interface for preparing Pickering emulsions. The morphology and rheological behavior indicated that the oil/water emulsion stability improved with the increasing mHNT concentration and milling time. SEM images showed that the emulsion network became denser with the increasing milling time of mHNTs, which led to the increased stability of the emulsions. In addition, the antibacterial properties of HNT–cassia oil emulsions were investigated. Owing to the uniform distribution and slow release of cassia oil, mHNT-stabilized emulsions exhibited improved antibacterial performance. This work demonstrated that hydrophobic HNTs prepared by ball-milling method show proper wettability, controlled delivery behavior, and scaling-up ability, which have promising applications in Pickering emulsions and food preservation.

**KEYWORDS:** halloysite, nanotubes, hydrophobization, Pickering emulsion, antibacterial activity



## 1. INTRODUCTION

Emulsion, a uniformly mixed dispersion system consisting of two immiscible phases, has a wide range of applications in the fields of food science,<sup>1,2</sup> personal care,<sup>3</sup> biomedicine,<sup>4</sup> and sewage treatment.<sup>5</sup> However, the dispersed oils in the continuous aqueous phase as tiny droplets drastically increases the interfacial area, resulting in thermodynamic instability of the whole system.<sup>6</sup> Therefore, in order to increase the system stability, traditional emulsions mainly use surfactants as emulsifiers to reduce the surface energy. Unfortunately, the industrial production of conventional emulsions leads to the extensive use of surfactants, which raises the issue of environmental hazards. As an alternative to surfactants, various solid particles have been developed as emulsifiers for emulsions, and these new types of emulsions are called Pickering emulsions. Compared to surfactants, the irreversible interfacial adsorption of solid particles endows the Pickering emulsion with high stability and high selectivity,<sup>7</sup> making the development of ecofriendly emulsion simple and accessible. Therefore, Pickering emulsions become one of the solution to global food safety problems. At present, there have been studies<sup>8,9</sup> using Pickering emulsion as an encapsulation system for the delivery of antibacterial drugs to solve the problems of low water solubility and high volatility of the drugs in food

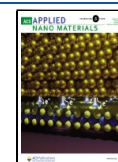
preservation. However, the choice of emulsifier is key to the successful preparation and functionalization of Pickering emulsions. To date, owing to the properties of being nontoxic, cheap, available, easy to store, and ecofriendly, solid particles such as inorganic particles, proteins, and polysaccharides have been studied widely as emulsifiers.<sup>2,10</sup>

As a natural inorganic material, clay has a wide range of applications in fields such as biomedicine, food science, environmental protection, and materials science due to its large reserves and safety nature.<sup>11–14</sup> Most clays are hydrated silicates containing metal ions such as aluminum (Al), zinc (Zn), magnesium (Mg), and iron (Fe).<sup>15</sup> Structurally, clays are layered minerals formed by combining silica–oxygen tetrahedra and aluminum or magnesium–oxygen octahedra in a 1:1 or 2:1 ratio through shared apical oxygen or hydroxyl linkages.<sup>16</sup> Based on their stable chemical properties, ecofriendliness, good biocompatibility, and unique structural

Received: June 2, 2022

Accepted: July 5, 2022

Published: July 18, 2022



morphology (e.g., montmorillonite in flakes, attapulgite in rods, and halloysite in tubes), a variety of clay particles have been used for the preparation of Pickering emulsions for different applications.<sup>17</sup> For example, Cheng et al.<sup>18</sup> prepared a 3-aminopropyltrimethoxysilane (APTMS)-grafted kaolinite sheet with enhanced emulsion stability by a microwave-assisted method and used it to stabilize Pickering emulsions in oil recovery operations. Nonetheless, probably owing to the lower specific surface area, the amount of oil stabilized by kaolinite was lower than that of other clays.<sup>19</sup> At the same time, the results showed that the higher specific surface area of halloysite nanotubes (HNTs) endowed them with better oil stabilization ability.

The chemical composition of HNTs is very similar to that of kaolin, which is a layered clay formed by alternately overlapping silicon–oxygen tetrahedral layers and aluminum–oxygen octahedral layers. The difference is that HNTs appear microscopically as a tubular structure in which flaky kaolin is rolled up. The outer silica–oxygen tetrahedral layer and the inner alumina–oxygen octahedral layer endow the HNTs with different inner and outer surface electrical properties, which facilitate the selective functionalization of different surfaces of HNTs by electrostatic adsorption. The large number of reactive sites on the surface and loadable lumens of HNTs have enabled the application of HNTs in the areas of biological interfaces<sup>20</sup> and antibacterial properties.<sup>21</sup> During the preparation and application of Pickering emulsions, wettability, size, surface properties, and concentration of emulsifier particles play a critical role.<sup>6</sup> It has been demonstrated that HNTs can be successfully used in the preparation of Pickering emulsions.<sup>22,23</sup> There have been considerable studies on loading chemicals into the lumen of HNTs or grafting them on the outer surface to prepare functional Pickering emulsions for different applications.<sup>24</sup> However, HNTs have good water dispersion ability, which is contrary to the moderate wettability required by emulsifier particles. Hence, this feature of HNTs leads to unsatisfactory emulsifying ability of raw HNTs during emulsification. Tailoring the wettability of HNTs becomes the key to enhance the emulsifying ability of HNTs. Polytetrafluoroethylene (PTFE) is one of the most commonly used polymers in medical devices due to its physical and chemical inertness, and it has good hydrophobicity.<sup>25</sup> Using PTFE to modify HNTs could be an effective way to tailor the wettability of HNTs.

In this work, the hydrophobic HNTs were successfully prepared by ball milling of HNTs in a PTFE jar, so that PTFE was transferred from the jar wall to the surface of HNTs during the milling process. A series of characterizations on the morphological structure and physicochemical properties of the hydrophobic HNTs were carried out to verify the size reduction of HNTs and the successful attachment of PTFE on the surface of HNTs. Different experiments were performed to examine the hydrophobicity of modified HNTs. Hexadecane, a common model oil, was selected as the oil phase of the emulsion to explore the distinction in the ability of HNTs with different degrees of modification to emulsify the oil phase. Based on the good emulsifying properties of the modified hydrophobic HNTs, cassia oil was then selected as the oil phase. *Staphylococcus aureus* (*S. aureus*) and *Escherichia coli* (*E. coli*) were used as model bacteria to explore the antibacterial properties of the cassia oil emulsion stabilized by hydrophobic HNTs. This work proposes a simple and green method for the hydrophobic modification of HNTs to improve the emulsifying

ability of the clay particles, which shows promising applications in biomedicine or food science.

## 2. EXPERIMENTAL SECTION

**2.1. Materials.** Purified HNTs were provided by Guangzhou Runwo Materials Technology Co., Ltd., China. Cassia oil (CAS: 8007-80-5, refractive index of 1.592, density of 1.03 g/mL) and hexadecane (CAS: 544-76-3, AR 98%) were purchased from Shanghai Macklin Biochemical Co., Ltd, China. Rhodamine B was purchased from Tianjin Tianxin Fine Chemical Development Center, China. Acridine orange/ethidium bromide (AO/EB) staining reagents were purchased from Beijing Solarbio Science & Technology Co., Ltd., China.

**2.2. Hydrophobic Modification of HNTs.** HNTs were modified by ball milling at room temperature with a planetary ball miller (QM-3SP4, CHISHUN TECH, Nanjing, China) at 300 rpm for different times (0.5, 1, 2, 3, and 4 h). The typical procedure was as below. 5 g of HNTs was added to a 500 mL PTFE ball mill jar (CHISHUN TECH, Nanjing) equipped with zirconia beads. The heat and shear force generated during the milling process activated PTFE of the jar walls. This caused PTFE to fall off and attach to the surface of the nanotubes for obtaining hydrophobized HNTs. Mill-modified HNTs were denoted as mHNTs in the text, and raw HNTs were denoted as rHNTs.

**2.3. Characterization of Modified HNTs.** Transmission electron microscopy (TEM) (JEM-1400F, JEOL Ltd., Japan) and scanning electron microscopy (SEM) (SU1000, HITACHI, Japan) were used to characterize the morphology of HNTs before and after milling. At least 100 particles of each sample in SEM images were counted by Image J software to analyze the changes in the average length and size distribution of HNTs. The zeta potential and particle size distribution were analyzed by Zetasizer Nano ZS (Malvern Instruments Co., UK). Samples were dispersed in deionized water or absolute ethanol before the testing. Fourier transform infrared spectra (FTIR) of HNTs were analyzed by a Thermo FTIR spectrometer (Nicolet550, Thermo Fisher Scientific Co., Ltd., USA) in the range of 4000 to 400  $\text{cm}^{-1}$ . The crystal structure of the samples was detected by an XRD instrument (MiniFlex-600, Rigaku Corporation, Japan) in the range of 5 to 70° with an accelerating voltage of 40 kV and a current of 40 mA. In order to study the effect of the milling process on the pore size distribution and specific surface area of HNTs, the  $\text{N}_2$  adsorption and desorption of rHNT and mHNT powders were analyzed by a specific surface area and pore size analyzer (Quantachrome Instruments, America). The surface elemental composition of mHNTs at 4 h was analyzed by field emission TEM with energy-dispersive X-ray spectroscopy (EDS), and the contents of C, O, Al, Si, and F were detected.

**2.4. Wettability of HNTs.** The effect of hydrophobic modification time on the water dispersion behavior of HNTs was investigated by shaking or ultrasonic dispersion of HNT powder in water. 0.1 g of rHNTs and mHNTs was added into small bottles containing 10 mL of water, respectively. The bottles were shaken slightly by hand for 15 s. For comparison, the bottles containing different HNTs were ultrasonically dispersed for 10 min by an ultrasonic cleaner (SK1200H, Shanghai Kudos Ultrasonic Instrument Co., Ltd., China). The water dispersion ability of HNTs treated with different methods was observed. In the ultrasonic dispersion group, the floated HNTs in the upper layer were removed by sieve filtration, and the remaining dispersion was dried to calculate the ratio. Each set of samples was measured at least three times.

Then, the water contact angle of HNTs before and after ball milling was examined. mHNTs (0.8 g) with different milling times were pressed into flakes, and their water contact angles were measured using a contact angle tester (DSA 100, DataPhysics, OCA-25, Kruss Co., Ltd., Germany). The contact angles were measured immediately after the deposition of droplets onto the HNTs flakes, and the changes in contact angles were also recorded at 10 s and 1 min. The volume of the water droplets was  $10.0 \pm 0.5 \mu\text{L}$ , and at least three measurements were performed for each sample.

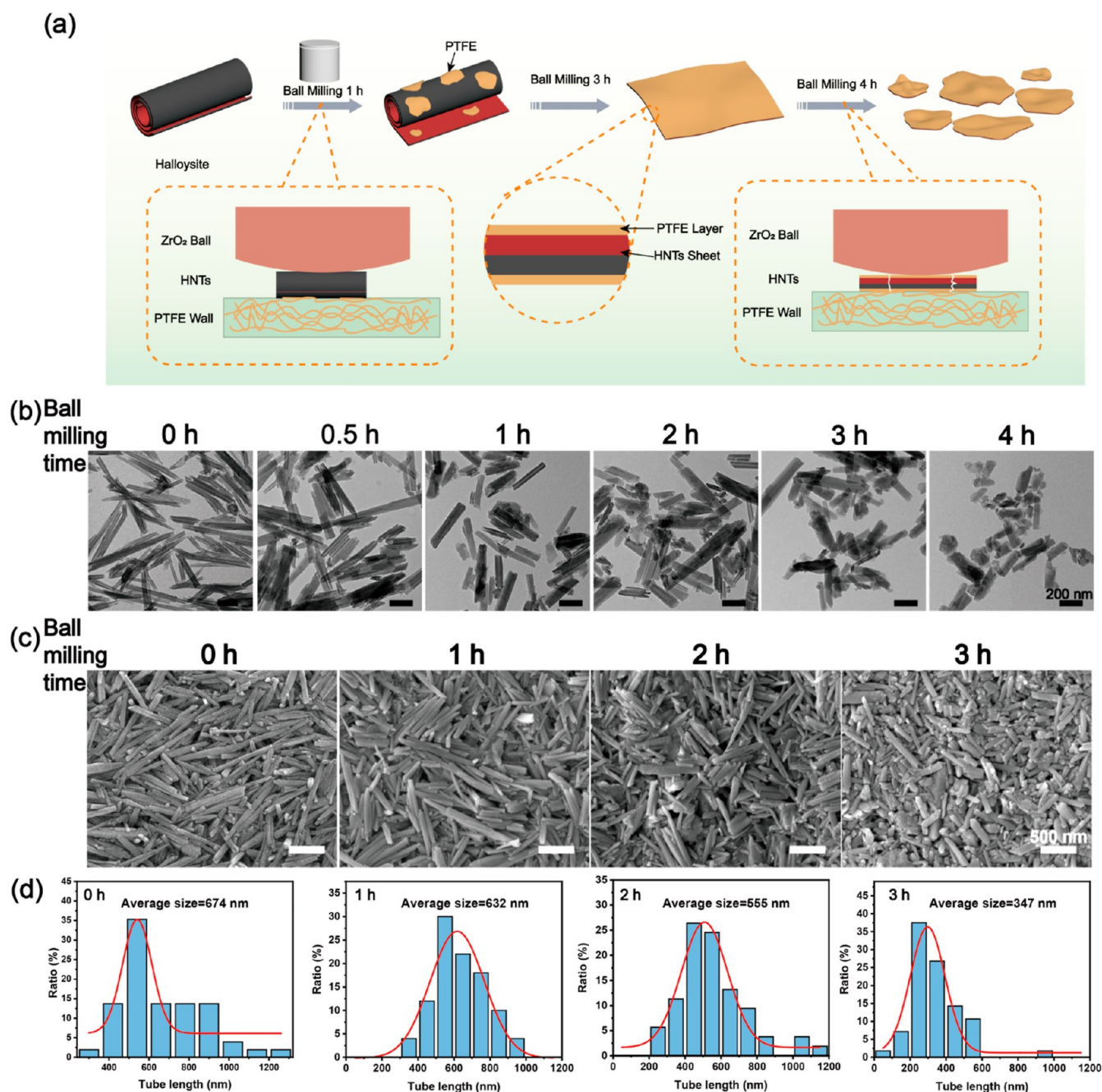


**Figure 1.** (a) Schematic illustration of the preparation of sheet-like and hydrophobic HNTs by ball milling. (b) TEM, (c) SEM, and (d) corresponding length distribution statistics of HNTs at different ball milling times.

Water droplets (10  $\mu\text{L}$ ) were rolled on mHNT powder to coat a layer of mHNTs. The states of the pellets on different materials were observed to evaluate the stability of the water droplets encapsulated by mHNTs in different media.

**2.5. Preparation of Hexadecane Emulsions Stabilized by mHNTs.** rHNTs were diluted with deionized water and prepared into suspensions with concentrations of 1, 2, 6, and 10 wt % for use. 4 mL of rHNT suspensions of different concentrations was mixed with 4 mL of hexadecane, and a Pickering emulsion with a water–oil ratio of 1:1 was obtained by ultrasonication in an ice bath using an ultrasonic cell disruptor (Xiaomei Ultrasonic Instrument (Kunshan) Co., Ltd., China) at a power of 500 W for 10 min. The mHNTs with different milling times were first dispersed in 4 mL of hexadecane and prepared into dispersions with concentrations of 1, 2, 6, and 10 wt %, respectively. Hexadecane containing mHNTs was mixed with 4 mL of deionized water and sonicated in an ice bath to form Pickering

emulsions. The prepared emulsions were allowed to stand at room temperature for 24 h for a series of characterizations.

**2.6. Characterization of Hexadecane Emulsions Stabilized by mHNTs.** Optical microscopy was used to observe the microstructure of different emulsions. The emulsion was diluted with water (1 mL of emulsion/10 mL of water) before observation. A small amount of the emulsion was dropped onto a microscope glass slide and covered with a coverslip for observation. For each sample, at least 100 droplets were analyzed with Image J software to obtain the mean droplet diameter and size distribution of the emulsion. The emulsifying ability of different HNTs was also evaluated by the creaming index (CI), which was defined as the ratio of the volume of the cream layer to the volume of the whole mixture. The rheological behavior of Pickering emulsions stabilized with different HNTs at 3% mass fraction was investigated by a rotational rheometer (Kinexus pro

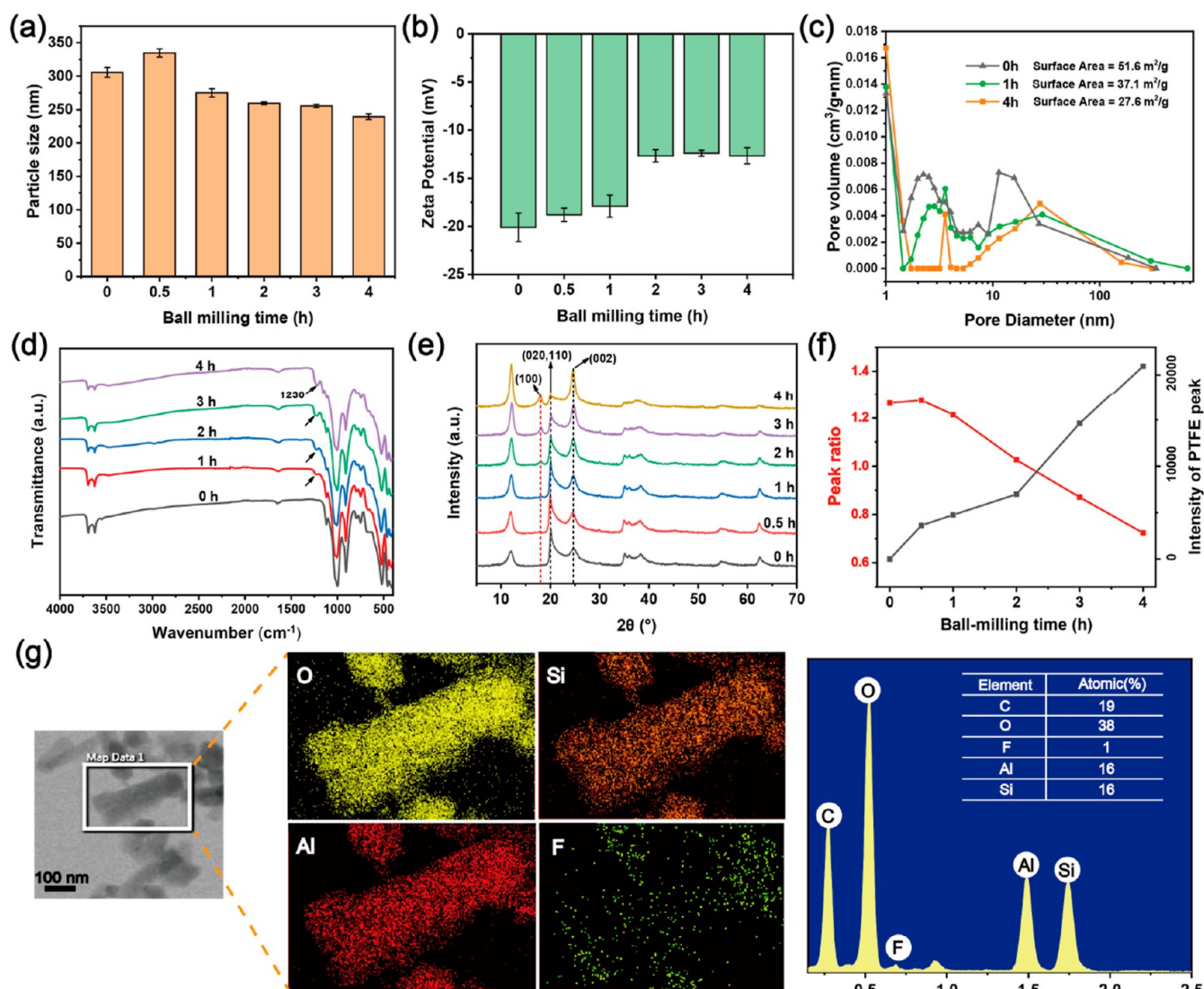


**Figure 2.** (a) Particle size, (b) zeta potential, (c) pore size distribution and surface area, (d) FTIR analysis, (e) XRD, (f) ratio of the diffraction intensities of (020, 110) and (002) planes and the intensity change of the PTFE peak of HNTs at different ball milling times, and (g) element distribution and TEM-EDS spectra of milling HNTs.

+, Malvern Instruments Co., Ltd., England) equipped with a 20 mm parallel plate model.

To show the localization of HNTs in the emulsion, fluorescence imaging of the emulsion was performed using a confocal laser microscope (Zeiss, LSM800, Germany). First, rHNTs and mHNTs at 1 and 4 h were stained with Rhodamine B in deionized water and absolute ethanol, respectively. The dyed HNTs were used to prepare a 1 wt % hexadecane Pickering emulsion (water/hexadecane (volume) = 9:1). 5  $\mu\text{L}$  of the emulsion sample was dropped onto a microscope slide and covered with a coverslip, and a 40 $\times$  oil microscope was used to observe at an excitation wavelength of 561 nm.

Field emission SEM (FE-SEM) (Zeiss, Sigma 300 Germany) was used to further observe the microstructure of the emulsions. rHNTs and mHNTs at 1 and 4 h were used to prepare Pickering emulsions with an emulsifier concentration of 3 wt % (water/hexadecane = 1:1). The cream layers of the emulsions after 24 h of resting were lyophilized for studying the morphology of the emulsion networks formed by different HNTs at different magnifications.

**2.7. Antibacterial Activity of Cassia Oil Emulsions Stabilized by HNTs.** mHNTs at 4 h were used to prepare cassia oil emulsions with concentrations of 0.5, 1, 3, and 5 wt %, while rHNTs were used to prepare cassia oil emulsions with a concentration of 5 wt %. The

formation of the cassia oil emulsion was similar with the preparation method of the hexadecane emulsion, but the oil–water ratio was set as 1:9. The inhibitory ability of cassia oil emulsion stabilized with different milling times and concentrations of HNTs against *S. aureus* and *E. coli* was evaluated by the agar disc diffusion method. Two strains were grown overnight in LB medium in a constant-temperature shaker at 37  $^{\circ}\text{C}$  with a shaking speed of 120 rpm. 5 mL of LB medium for both strains was added to 100 mL of warm agar medium and then was quickly poured into sterile Petri dishes after mixing well by shaking. After the agar medium solidified, sterilized paper plates with 6 mm diameter were placed onto the agar plates under aseptic conditions. 10  $\mu\text{L}$  of deionized water, cassia oil–water mixture (cassia oil/water = 1:9), cassia oil emulsion stabilized with different HNTs, and 0.5 mg mHNTs were added to the paper discs. Deionized water and mHNTs were autoclaved before being added to the filter paper. Petri dishes were incubated in a constant-temperature incubator at 37  $^{\circ}\text{C}$  for 24 h, and then the size of the inhibition circle diameter was measured. At least three parallel sets of tests were done for each sample.

The bacterial inhibition rate of different samples over time was also evaluated in LB medium to further assess the antibacterial properties of the emulsions. *S. aureus* and *E. coli* were incubated in LB medium in a constant-temperature shaker at 37  $^{\circ}\text{C}$  for 12 h at 120 rpm. The

overnight culture broth was diluted with LB medium to a bacterial concentration of approximately  $10^6$  CFU/mL. 8  $\mu$ L of cassia oil, 80  $\mu$ L of sterile water, 4 mg of mHNTs, 5 wt % rHNTs, 0.5 wt % mHNTs, and 5 wt % mHNT-stabilized cassia oil emulsion were added to 8 mL of diluted bacterial solution, respectively, making the final concentration of cassia oil of 1  $\mu$ L/mL. The mixed bacterial solution was placed in a constant-temperature shaker at 37  $^{\circ}$ C to co-incubate with the material. 200  $\mu$ L of bacterial solution was taken in a 96-well plate at different incubation times (measured every hour for 6 hours) to test its absorbance value by an enzyme marker (BioTek, Cytation 3, America) at 600 nm. The bacterial inhibition rates were calculated using the following equation

$$\text{Inhibition rate (\%)} = \frac{A_C - A_S}{A_C} \times 100\%$$

where  $A_C$  is the increase in absorbance of the sterile water group at different times relative to that at 0 h, and  $A_S$  is the increase in absorbance of the experimental groups relative to that at 0 h.

Live/dead bacterial viability assay was used for visualizing the antibacterial properties of emulsions against *S. aureus* using a mixture of green AO and red EB fluorescent dyes.<sup>26</sup> 4 mL of *S. aureus* solution at a concentration of  $10^8$  CFU/mL was used for co-incubation with 40  $\mu$ L of different samples (PBS, 10% cassia oil water mixture, 5 wt % rHNTs, and mHNTs stabilized with cassia oil emulsion). At different incubation times (1, 2, and 6 h), 1 mL of the samples was removed and subjected to centrifugation to remove the medium, followed by the addition of 100  $\mu$ L of AO/EB staining solution (1:1:50) and left to stain for 20 min in the dark. After centrifugation to remove the dye solution, the bacteria were washed twice with PBS. The bacterial solution resuspended in 1 mL of PBS buffer was dropped on the glass slide, covered with a coverslip, and the confocal microscope was used to observe the bacteria.

### 3. RESULTS AND DISCUSSION

**3.1. Morphology Characterization of HNTs.** Figure 1a shows the schematic of hydrophobic modification and ball milling process of HNTs. As shown in the figure, the HNTs were ground in a PTFE jar, causing them to be gradually crushed and flattened under shearing by the zirconia balls. Meanwhile, PTFE was gradually activated and dropped to attach to the surfaces of HNTs under the impact effect. With the increase of the milling time, 1D HNTs were gradually transferred into 2D flakes, and PTFE attached to HNTs gradually increased. After 4 h of milling, the PTFE-adhered HNTs were broken into smaller pieces. To verify the morphological changes of HNTs that occurred during the ball milling process, TEM and SEM were used to observe their surface morphology. As shown in Figure 1b, the TEM images of HNTs at different milling times were characterized. The rHNTs showed a clear lumen, while the walls of the tube collapsed, and some lumen of some mHNTs disappeared after milling for 1 h. Part of HNTs were destroyed during the milling process, so that the tube-like structure changed to a sheet-like structure. With the increase of milling time, the proportion of sheet structures gradually increased, while the size of nanosheets gradually decreased. The SEM images of HNTs in Figure 1c showed similar results. The length of the tube decreased and the width of the tube increased. The length statistics of HNTs in Figure 1d revealed a pattern of decreasing HNTs size with the ball milling time. For example, the average size of mHNTs at 3 h was 347 nm, which was 327 nm less than that of the rHNTs. Further increasing the milling time or increasing the milling power will increase the fragmentation degree of the nanosheets and lead to aggregation.

**3.2. Characterization of the Physicochemical Properties of HNTs.** The physicochemical properties of the modified HNTs were then analyzed. Figure 2a shows the change of the average particle size of HNTs during the milling process. The average particle sizes of HNTs reduced from 336 to 239 nm after 4 h of milling. The continuous decline of the size with the increase of the milling time verifies that the mechanical force of ball milling reduced the size of HNTs. The destruction of the lumen of HNTs by milling and the covering of PTFE caused some changes in the chemical properties of HNTs as well. The change in the potential of HNTs during milling could be attributed to the coverage of electrically neutral PTFE, which increased the potential of negatively charged HNTs from  $-20.1$  to  $-12.4$  mV (Figure 2b). In addition, the pore size distribution of HNTs (Figure 2c) also confirmed the changes that occurred during the milling process. The rHNTs had pore sizes in the 2–3, 10–20, and 50 nm regions corresponding to the surface pores, lumens of the tubes, and gaps formed by the lap between tubes, respectively. It could be found that the peak intensity of mHNTs at the 2–3 nm position declined after 1 h of milling, and this peak further disappeared after 4 h of milling, which was attributed to the filling of the pores by PTFE when PTFE covered the surface of HNTs. Simultaneously, the peaks at 10–20 nm showed a decreased trend, which was explained by the destruction of the HNT lumen and the formation of nanosheets during the ball milling process.

To characterize the adhesion of PTFE on the surface of HNTs, FTIR and XRD were used to characterize the changes in the chemical composition of the modified HNTs. Compared to the spectra of rHNTs, the FT-IR spectroscopic analysis (Figure 2d) of mHNTs revealed the successful loading of PTFE on the HNT surfaces by the new peaks at around 1230  $\text{cm}^{-1}$  that were characteristic of the C–F stretching bands of PTFE. As showed in Figure 2e, the XRD peaks of raw HNTs mainly appeared at 7.3  $\text{\AA}$  (001 plane), 4.5  $\text{\AA}$  (020, 110 plane), and 3.6  $\text{\AA}$  (002 plane). After milling, the peak intensity of the (202, 110) crystal plane related to the characteristic of tubular halloysite decreased obviously, which can be considered to be caused by the increased disorder of mHNTs due to the destruction of the lumen.<sup>27,28</sup> Furthermore, compared with rHNTs, mHNTs showed an additional peak at  $2\theta = 18.2^{\circ}$ , which was attributed to the (100) crystal plane of PTFE.<sup>29</sup> The relationship between the ratio of the diffraction intensity of the (020, 100) crystal plane to the diffraction intensity of the (002) crystal plane and the milling time was analyzed in Figure 2f. There was a downward trend toward the peak intensity ratio with the increase of the milling time, meaning the rise in the degree of structural disorder of the mHNTs. On the contrary, the intensity of the PTFE peak showed an increasing trend, indicating that the adhered PTFE increased with the milling time.

In order to further verify the cover of PTFE on the HNT surface, EDS was exerted to analyze the surface elements of mHNTs. As a natural aluminosilicate, HNTs contain only aluminum, silicon, and oxygen as elements. However, Figure 2g shows a fluorine signal in the EDS spectra of mHNTs, indicating the presence of PTFE. From the element mapping of mHNTs, it was observed that the green dots (F element) were only distributed where the mHNT sheets were located, which demonstrated that PTFE was localized on the mHNT surface rather than mixed in the mHNT powder. To determine the loading of PTFE on mHNTs after 4 h of milling, the thermal decomposition process of mHNTs was investigated.

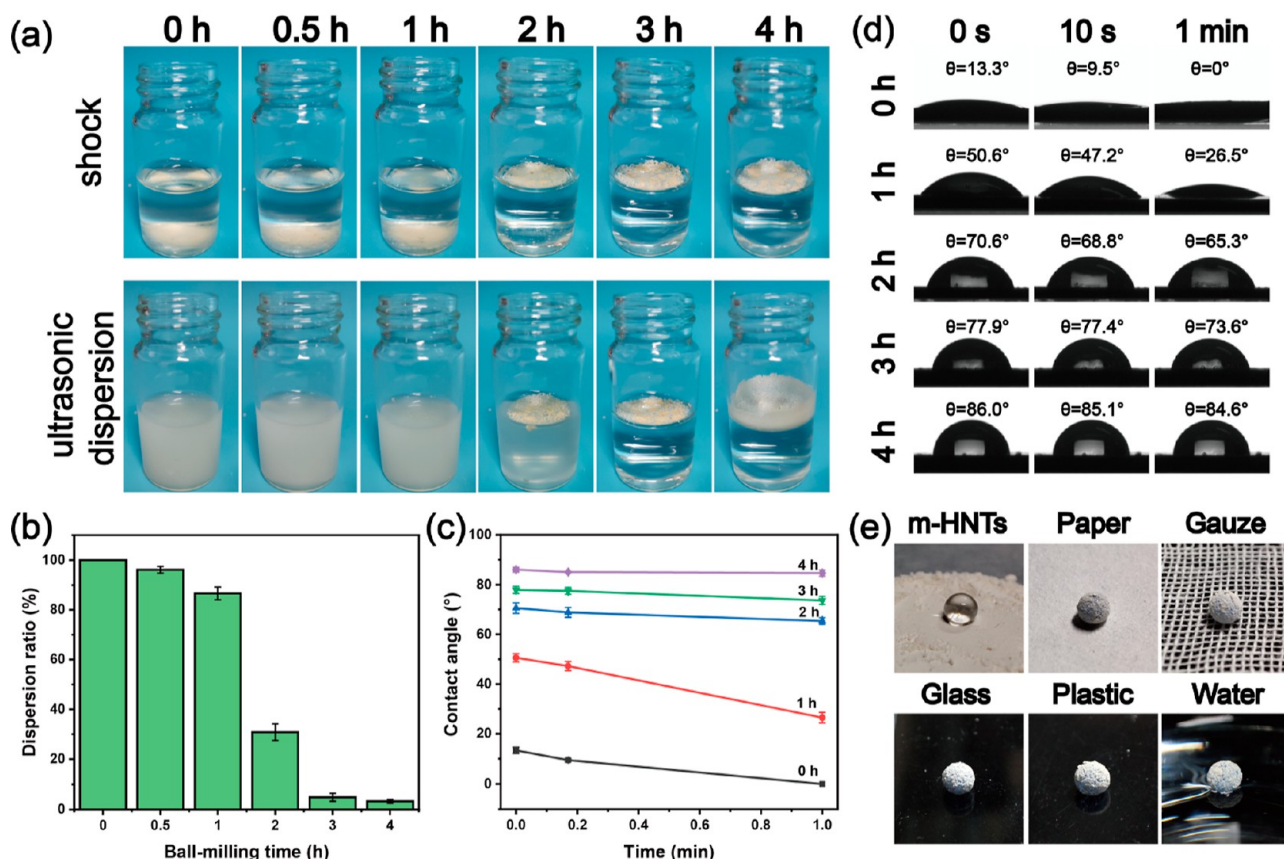


**Figure 3.** (a) Dispersion ability of HNTs under different conditions, (b) corresponding dispersion ratio statistics, (c) static contact angle statistics, and (d) contact angle image at different times of HNTs with different ball milling times; (e) images of water droplets on the mHNT powder, and water droplets wrapped with mHNT powder on the surfaces of paper, gauze, glass, plastic, and water.

The TGA curves (Figure S1) showed the thermal weight loss rate of 100% for PTFE, 20.9% for pure HNTs, and 27.1% for mHNTs, which indicated that the mass ratio of PTFE in the composite was 6.2%. These results indicated that PTFE was successfully attached to the HNTs surface during the milling process, and the amount of PTFE on the HNT surface increased with the increasing milling time.

**3.3. Hydrophobic Performance of HNTs.** rHNTs were hydrophilic due to the hydroxyl groups on the inner and outer surfaces of HNTs, which allowed them to disperse well in water and settle after a period of time. In contrast, the mHNTs adhered by PTFE during the milling process exhibited marked hydrophobicity. The hydrophobicity of mHNTs was caused by the attachment of PTFE molecular chains during the ball milling process. Because the inner lumen of HNTs has numerous hydroxyl groups, the exposure of the inner surfaces after the destruction of the lumen will not cause a change in hydrophobicity. As shown in Figure 3a, the rHNTs would sink to the bottom of water after slight shaking and could be completely dispersed in water after dispersion using the ultrasound machine. After milling, the mHNTs at different milling times exhibited varying hydrophobicity. Most of the mHNTs within 1 h of milling sank to the bottom of water after shaking, and the remaining small portion floated on the water surface. A minor amount of mHNTs could not be dispersed in water even after ultrasonic dispersion. After milling for more than 2 h, the mHNTs exhibited an apparent repulsion to water. Most of the mHNTs floated on water after shaking, and these

mHNTs could not be dispersed in water even after ultrasonic treatment. In order to analyze the effect of milling time on the hydrophobicity of mHNTs, the water dispersibility of mHNTs after ultrasonication was calculated. The water dispersibility of mHNTs milled for less than 1 h did not have significant changes, which was caused by less PTFE adhesion due to the shorter milling time. In contrast, mHNTs with 2 h of milling had a significantly decreased water dispersibility of 30.8%. The water dispersibility of mHNTs fell precipitously to as low as 3.33% when the milling time was longer than 3 h. The difference in water dispersibility between mHNTs milled for 3 and 4 h was not significant, probably because most of the HNT surfaces had been wrapped by PTFE, and the thickening of the PTFE layer did not result in significantly greater hydrophobicity.

To further investigate the effect of milling on the hydrophobicity of HNTs, the dynamic water contact angles of HNTs with different degrees of modification were measured. The results (Figure 3c,d) show that the water contact angle increased markedly with the increase of milling time. The instantaneous contact angle increased from 13.3° of rHNTs to 86° after 4 h of milling in a PTFE jar. It could be found that the loading of PTFE had a great influence on the dynamic contact angle of HNTs. The water contact angles of rHNTs varied greatly with time, and the water droplets were completely absorbed by the clay within 1 min. In contrast, mHNTs with a milling time of more than 2 h had a more stable water contact angle, and the stability of the contact angle

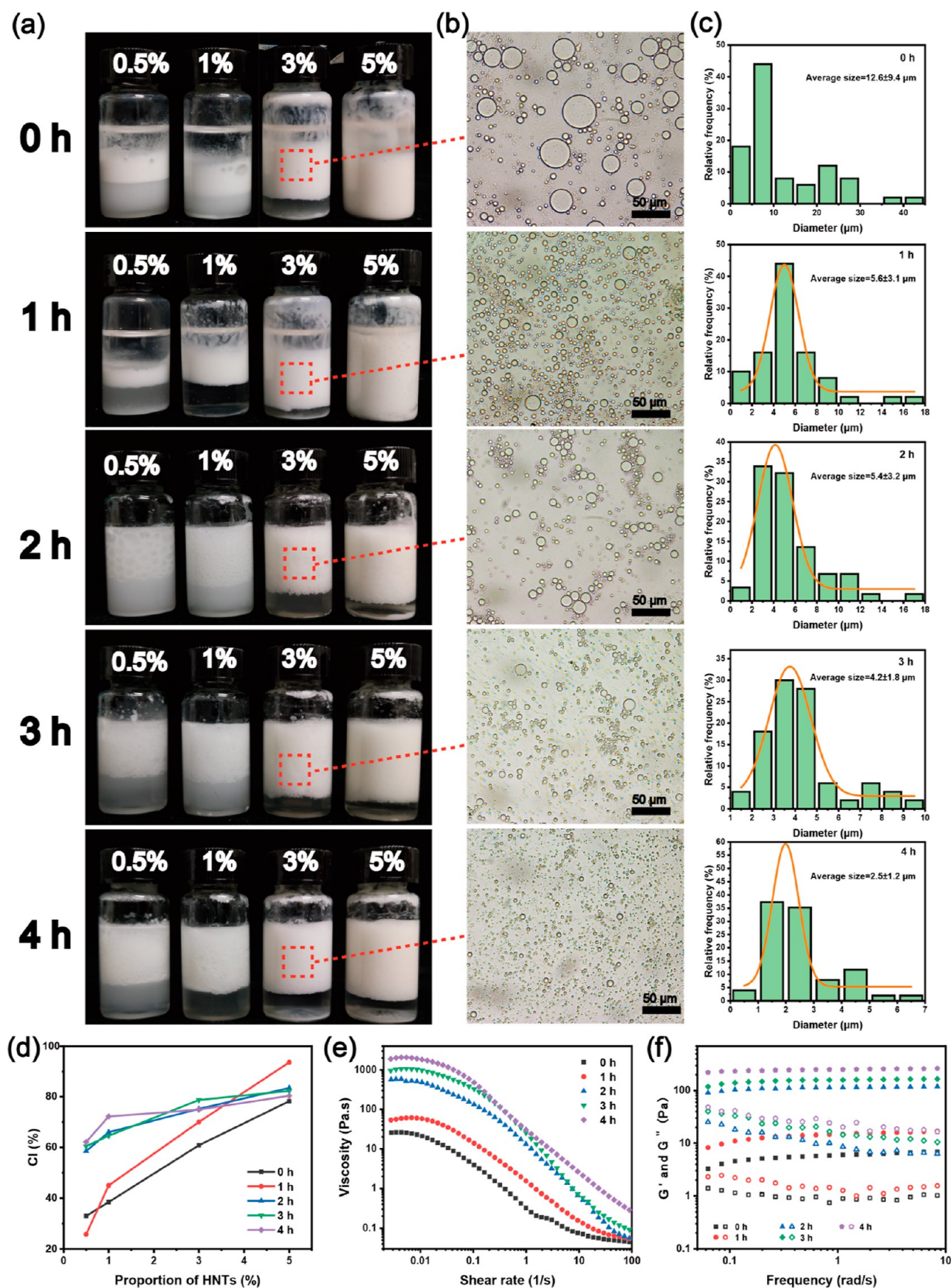


**Figure 4.** (a) Photographs, (b) optical microscope images, (c) droplet size distribution, (d) CI and rheological properties of (e) apparent viscosity and (f)  $G'$  (closed symbols) and  $G''$  (open symbols) of hexadecane emulsions stabilized by different concentrations of HNTs at different milling times.

increased with the increase of the ball milling time. The phenomenon could be explained by the increase of the PTFE amount on the surfaces of the HNTs as the milling time increased. Less water could be in direct contact with the mHNT surface, leading to a gradually improving stability of the contact angle. Almost constant dynamic water contact angle also proved the presence of PTFE layer on the surfaces of HNTs, and the polymer layer was stable and would not fall off.

Interestingly, a layer of mHNTs was assembled on the surface of the water droplets when they were dropped and rolled on the mHNT powder after 4 h of milling. As shown in Figure 3e, this shell of mHNTs enabled the water droplets to “stand” stably on filter paper, gauze, plastic, glass, and water, indicating that mHNTs could stabilize the water droplets between different interfaces.

**3.4. Performance of HNTs in Stabilizing Hexadecane Emulsion.** Previous studies<sup>24,30</sup> suggested that the wettability of nanomaterials determined the type of water–oil emulsion (W/O or O/W). In addition, the surface charge of the adsorbed particles is also an essential parameter to control the stability of Pickering emulsion. The hydrophobicity of the PTFE-modified HNTs was increased, which gave it suitable wettability. During the formation of Pickering emulsions, a suitable wetting angle facilitates the adsorption of nanoparticles at the oil/water interface, forming steric hindrance to prevent the coalescence of oil droplets in the Pickering emulsion. The low surface charge of mHNTs was beneficial to promote the coalescence and aggregation of particles at the interface, which was more suitable for the stabilization of Pickering emulsion. In addition, it has been demonstrated<sup>31</sup> that solid particles in the form of flakes also have good emulsification ability. Therefore, Pickering emulsions were prepared using varying mass fractions of mHNTs at different milling times. Hexadecane, a nonpolar alkane with moderate carbon chain length and high stability, is a standard oil suitable for emulsification experiments and was used to investigate the emulsification ability of mHNTs.

Figure 4a shows the images of Pickering emulsions with different emulsifier concentrations prepared by HNTs at different milling times after 24 h of standing. It was found that only a small amount of oil was emulsified in the hexadecane emulsion used rHNTs as the emulsifier, and much of the oil was left at the top of the liquid. Even if the concentration of rHNTs was increased, it could not completely stabilize all the oils. On the contrary, the hydrophobically modified mHNTs showed stronger ability to stabilize oil. For emulsions prepared by mHNTs milled for 1 h, the amount of oil stabilized by mHNTs increased with the concentration of mHNTs in the system. mHNTs milled for more than 2 h were able to stabilize almost all the oil in the system.

The microstructure of the emulsions was subsequently studied by optical microscopy. Figure 4b,c show the microscopic images of the emulsions stabilized with different HNTs at 3% mass fraction and the corresponding droplet size distribution statistics. Compared to the emulsions prepared by rHNTs, the emulsions stabilized by mHNTs exhibited much smaller average droplet diameters (from  $12.6 \pm 9.4$  to  $2.5 \pm 1.5 \mu\text{m}$ ) and a more uniform droplet size distribution. At the same time, the average diameter of emulsion droplets exhibited a regular decrease with the increase of milling time. These results demonstrated that the hydrophobically modified HNTs adsorbed more at the oil–water interface due to their suitable

wettability and electrical properties, effectively inducing the formation of smaller emulsion droplets to increase the emulsion stability. The stability of the emulsions was assessed by the cream volume proportion calculated as CI, defined as

$$\text{Creaming index (CI)} = \frac{h_e}{h_t} \times 100\%$$

where  $h_e$  is defined as the volume of the emulsion layer after stratification due to gravity, and  $h_t$  is the total volume of the sample. The higher the CI, the more stable the emulsion.<sup>32</sup>

As shown in Figure 4d, the CI of all emulsions increased with the increasing concentration of HNTs. For rHNTs, the emulsifier concentration had a greater effect on the CI of the emulsions, with the CI only 33% at 0.5 wt % and rising to 78% at 5 wt %. However, all mHNTs had greater CI than rHNTs at particle concentrations greater than 1 wt %, and emulsions of mHNTs with milling times greater than 2 h had similar CI at different concentrations, indicating that hydrophobically modified HNTs show enhanced emulsion stabilization and that the ability to stabilize emulsions improves with the increasing hydrophobicity. The stability of the emulsion was also illustrated by the appearance of the emulsion after standing for 3 months. As shown in Figure S2, the emulsions stabilized by HNTs with a milling time higher than 2 h did not show demulsification and did not show any change in the emulsion layer height. In contrast, the rest of the HNT-stabilized emulsions had an oil phase observed at the top of the system, indicating that the emulsions prepared with longer milling times of mHNTs were more stable.

The rheological properties of Pickering emulsions were related to the appearance, processability, and stability of the emulsions.<sup>33</sup> The viscosity of emulsions at low shear rates is a parameter to characterize the stability of emulsions. To investigate the effect of hydrophobic modification of HNTs on the viscosity of the formed emulsions, the viscosity variation of the emulsions prepared by 3 wt % HNTs at different milling times was tested in the shear rate range of  $10^{-3}$  to  $100 \text{ s}^{-1}$ . As shown in Figure 4e, the viscosity of all emulsions declined with the increasing shear rate, exhibiting a typical shear thinning behavior, which implied that the emulsion network was disrupted with the increasing shear force. In addition, all the emulsions exhibited a plateau shear viscosity at low shear rates, which was defined as zero shear viscosity. It was found that the emulsions prepared by mHNTs at 4 h had the highest zero shear viscosity, which might be due to the fact that smaller droplets lead to tighter accumulation and less mobility, leading to the higher viscosity of emulsions.<sup>34</sup> Figure 4f shows the storage modulus ( $G'$ ) and loss modulus ( $G''$ ) as the functions of frequency for the emulsions prepared with 3 wt % HNTs. The results showed that the storage modulus for all emulsions was larger than the loss modulus, indicating that elasticity plays a dominant role in the emulsion, which exhibited a solid gel-like behavior on a macroscopic scale.  $G'$  and  $G''$  of the emulsions increased significantly with the increase of the milling time of HNTs.  $G'$  of mHNT emulsions with milling time greater than 2 h was an order of magnitude larger than that of rHNT emulsions due to the increased ability of these mHNTs to stabilize oil in the system. The high oil content led to a progressively closer and higher packing density of Pickering emulsion droplets, resulting in higher  $G'$  values.<sup>35</sup> In addition,  $G'$  and  $G''$  exhibited a weak correlation with frequency, which suggested that the emulsion system had

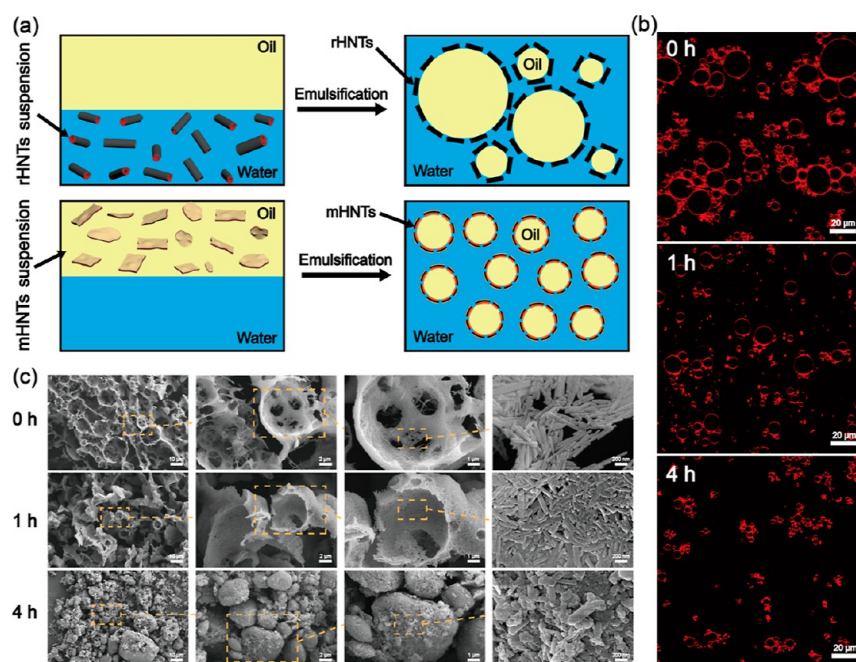


**Figure 5.** (a) Schematic illustration of the formation of hexadecane emulsion using rHNTs and mHNTs; (b) fluorescence micrographs and (c) SEM images of freeze-dried hexadecane emulsions stabilized by HNTs at different milling times.

significant gelation behavior and three-dimensional network.<sup>36</sup> The rheological properties of the emulsions indicated that the emulsions prepared by hydrophobically modified HNTs exhibited increased stability with milling time.

**3.5. Analysis of Emulsion Formation Mechanism.** The emulsion formation mechanisms of different hydrophobic HNTs were then investigated. As shown in Figure 5a, rHNTs were dispersed in aqueous solutions before emulsion formation due to their good water solubility. The high hydrophilicity of rHNTs allowed them to be mostly present in the aqueous phase, with only a small fraction being in contact with the oil droplets at the water–oil interface for emulsification. Thus, rHNTs induced the formation of larger oil droplets during emulsion formation, while forming a loose and porous layer of HNTs on the surfaces of the oil droplets. In contrast, mHNTs were hydrophobic, which resulted in a larger wetting angle to the oil phase. The mHNTs disperse in the oil phase before the emulsion formation and then migrate to the oil–water interface under the action of mechanical force to form a homogeneous and stable emulsion. However, the poor wettability of mHNTs to water resulted in the overall presence of mHNTs in the oil phase and only a small portion of them in contact with the water phase. Therefore, small emulsion droplets and a dense mHNT layer on the surface were formed. Earlier studies<sup>24,37</sup> have shown that the adsorption of interfacial particles is a key parameter for the stabilization of Pickering emulsions. Theoretically, when  $\theta = 90^\circ$  of the solid particle, its desorption from the interface requires the highest desorption energy. The appropriate wetting angle of mHNTs endows them with high desorption energy at the oil–water interface, making them irreversibly anchored at the interface. As a result, mHNT emulsions have higher stability than rHNT emulsions.

To verify the mechanism of emulsion formation, different HNTs (rHNTs and mHNTs at 1 and 4 h) were stained with Rhodamine B and prepared into emulsions using hexadecane as the oil phase. The position of HNTs in the emulsions was

subsequently visualized by CLSM. As seen in Figure 5b, all three emulsions showed strong red fluorescence on the surface of the emulsion droplets, and there was also a clear red fluorescence around the aggregation of the droplets, which indicated the presence of HNTs at the oil–water interface for oil droplet stabilization in the emulsions. Similar to the results obtained from the optical microscopy analysis, the average droplet size and size distribution of the three emulsions were distinctly different. The emulsions prepared by rHNTs exhibited a high average droplet diameter as well as size distribution. In contrast, the average diameter and size distribution of the emulsion droplets of mHNTs emulsion after hydrophobic modification decreased with the increasing milling time. The size of Rhodamine B-dyed emulsion droplet was slightly different from the result shown in Figure 4b, which was induced by the changed emulsifying ability of mHNTs by the loading of dyes.

To further confirm that HNTs were present at the water–oil interface to stabilize the emulsions, different emulsions with 5 wt % of the emulsifier were freeze-dried and observed by SEM. It was found in Figure 5c that the freeze-dried emulsions stabilized by rHNTs were left with a loose and porous rHNT skeleton, in which spherical shells composed with the tubular particles were clearly visible. During the freeze-drying process, the removal of both water and oil from the emulsion caused the three-dimensional network formed by HNTs to partially collapse, while retaining a part of the original structure. These spherical shells composed with tubular HNTs indicated that the nanotubes were present at the oil–water interface and wrapped around the outside of the oil droplets to form a protective layer. A large amount of HNTs formed a three-dimensional network to support the oil droplets and stabilize the emulsion. Compared to rHNTs, the emulsion of mHNTs at 1 h formed an apparently denser HNTs skeleton with fewer pores in the HNTs network skeleton. The presence of spherical shells with smaller diameter and size distribution demonstrated that the modified HNTs could induce the

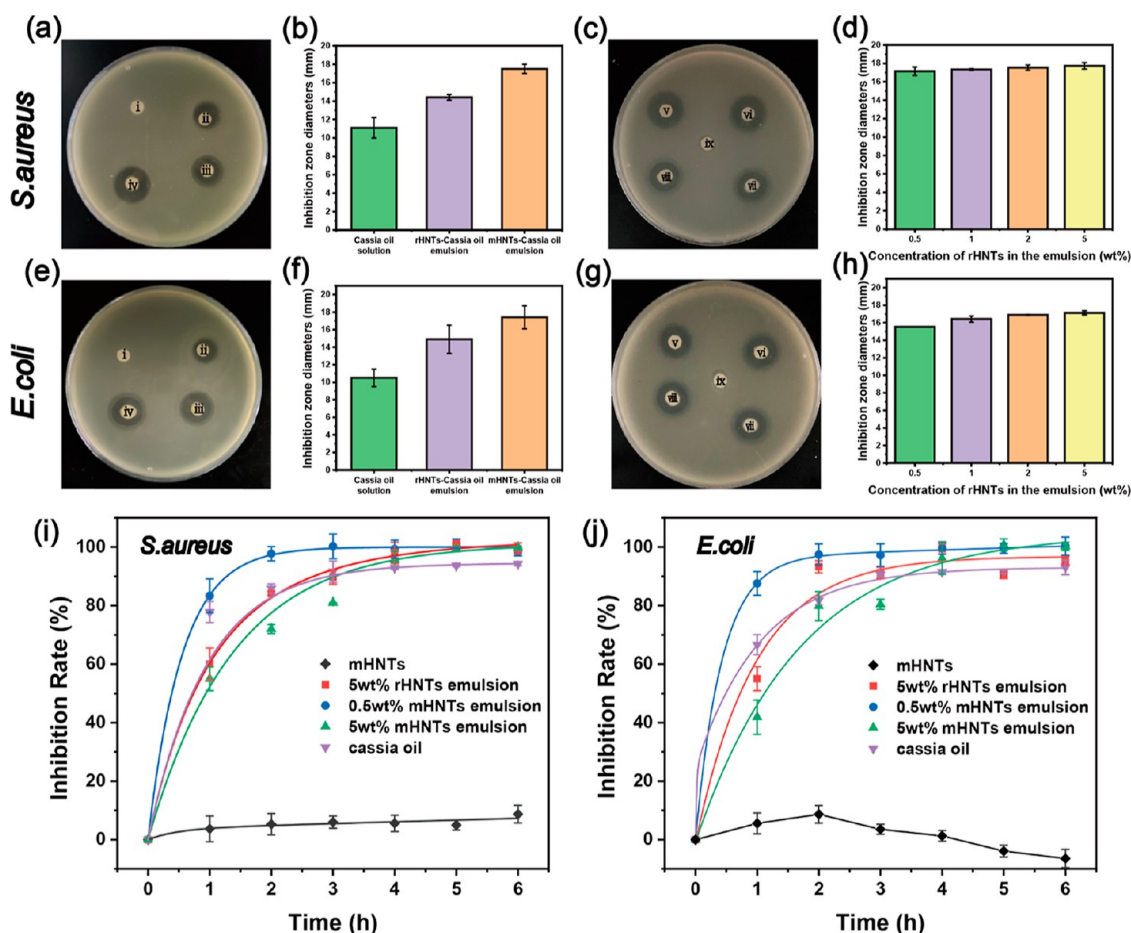


**Figure 6.** Photos and diameters of inhibitory zones against (a–d) *S. aureus* and (e–h) *E. coli* using (i) mHNT powder, (ii) cassia oil/water mixture (water-to-oil ratio, 9:1) emulsion stabilized with (iii) 5 wt % of rHNTs and (iv) 5 wt % of mHNTs; and emulsions stabilized with different concentrations of mHNTs ((v) 0.5 wt %, (vi) 1 wt %, (vii) 2 wt %, (viii) 5 wt %, and (ix) blank filter paper). Antibacterial rate of cassia oil, mHNT powder, and cassia oil emulsions stabilized with 5 wt % rHNTs and mHNTs against (i) *S. aureus* and (j) *E. coli* in LB medium.

formation of smaller emulsion droplets, which was consistent with the results obtained from the optical microscopy analysis. As for the emulsion prepared by mHNTs at 4 h, no sparse and porous skeleton of mHNTs were observed after freeze-drying, but small sphere-shaped aggregates were formed. The hydrophobicity of mHNTs led to a higher contact angle in the aqueous phase than in the oil phase. Thus, mHNTs could not be dispersed in the aqueous phase to form a skeleton, but gathered on the surfaces of the oil phase to form a thick shell consisting of mHNTs.

**3.6. Antibacterial Properties of Cassia Oil Emulsion Stabilized by mHNTs.** The afore-mentioned experiments using hexadecane as the oil phase demonstrated that hydrophobically modified HNTs have improved emulsification ability and used to prepare emulsions with improved stability, which made mHNTs valid candidates as emulsifiers for other oils (e.g., xylene, methylene chloride, and olive oil) for environmental remediation and drug delivery. Essential oils are aromatic liquids found in nature and are often used as food preservatives because of their antioxidant properties.<sup>38</sup> Cassia oil is recognized as a harmless essential oil with excellent antioxidant and antimicrobial properties,<sup>39</sup> which has promising applications in biomedical, pharmaceutical, and food fields. However, the undesirable properties of cassia oil such as insolubility in water and volatility limited its application.<sup>40</sup> mHNTs as emulsifiers to prepare O/W Pickering emulsions

for the encapsulation of hydrophobic cassia oil may be an effective way to solve the undesirable properties of cassia oil.

mHNTs were used to stabilize cassia oil in water, and the antibacterial ability of cassia oil emulsions was investigated in detail. The antibacterial activity of cassia oil emulsions stabilized by HNTs before and after modification was evaluated by the agar well diffusion method using *E. coli* and *S. aureus* as model bacteria with reference to a previous work with slight modifications.<sup>9</sup> Figure 6a,b shows the formation of inhibition zones induced by different materials (mHNTs, cassia oil, 5 wt % rHNTs, and mHNT emulsion) on agar plates containing *S. aureus* and the corresponding inhibition zone diameter statistics. Apparently, the mHNT powder used as a control had no significant inhibitory effect on the growth of *S. aureus*. This was because the natural clay of HNTs and the PTFE polymer were chemically inert and had no effect on bacterial growth. In contrast, all experimental groups containing cassia oil exhibited significant inhibition zones. The mixture of water and cassia oil without any emulsifier induced the production of inhibition zones with an average diameter of 11.1 mm on agar plates. Compared to the water-cassia oil mixture, cassia oil emulsions using HNTs as emulsifiers had stronger bacterial inhibition. The rHNT and mHNT emulsions resulted in inhibition zones with average diameters of 14.4 and 17.5 mm, respectively.

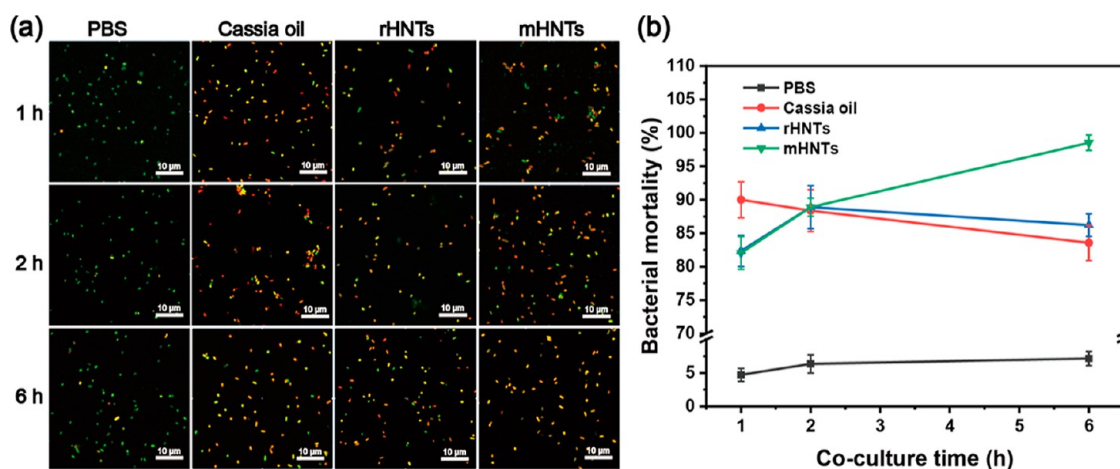


**Figure 7.** (a) Fluorescence images and (b) corresponding bacterial mortality data statistics of *S. aureus* co-cultured with different materials (PBS, cassia oil, rHNTs, and mHNTs).

Attributed to the hydrophobicity of cassia oil, pure cassia oil was difficult to be diffused on hydrophilic agar plates, leading to its reduced bacterial inhibition rate. However, by using mHNTs as emulsifiers to prepare cassia oil emulsion, the diffusivity of hydrophobic cassia oil on a hydrophilic medium was greatly improved, resulting in a significant expansion of the inhibition zone. mHNTs play the role of emulsifiers in the system, so that cassia oil can be uniformly dispersed in the aqueous solution to improve its antibacterial properties. In addition, translucent “ghost areas” at the edge of the inhibition zones were noticed, which consisted of fragments of dissolved bacteria colonies.<sup>41</sup> This phenomenon was caused by the slower diffusion of the bactericides, which could be explained by the slow release of cassia oil from the shell layer of HNTs. Compared to mHNTs, rHNT emulsion triggered slightly smaller inhibition zones, which were due to the poor ability of rHNTs to emulsify oil. Slightly lower cassia oil content was in the rHNTs emulsion compared to the mHNT emulsion. The antimicrobial ability of cassia oil emulsions stabilized with different concentrations of mHNTs was also evaluated (Figure 6c,d). It was found that the emulsions of cassia oil stabilized with different concentrations of mHNTs induced inhibition zones with comparable diameters, which proved that they had similar antibacterial ability. However, the transparency of the “ghost zone” of the emulsions with different concentrations of mHNTs decreased with the increase of the mHNT concentration. This might be due to the different thicknesses of the outer mHNT shell layer of the emulsion droplets, resulting in different release rates of the cassia oil. As the concentration of mHNTs increased, the layer of mHNTs encapsulating the cassia oil in the emulsion thickened, resulting in a slower release of cassia oil from the emulsion.

The same experiments were also carried out using *E. coli* as a model to verify that the emulsions had similar inhibitory effects on *E. coli*. The inhibition zones induced by the cassia oil emulsion on agar plates containing *E. coli* (Figure 6e–h) showed similar results to those of the *S. aureus* group, which demonstrated that the cassia oil emulsion prepared with HNTs as emulsifiers also had the same inhibitory effect on *E. coli*.

The antibacterial properties of the emulsions were also evaluated by bacterial growth kinetics to investigate the effect of HNT encapsulation on the bacterial inhibition ability of cassia oil. The inhibition rates of *S. aureus* and *E. coli* co-cultured with mHNTs, cassia oil, and different emulsions

over time are shown in Figure 6i,j. It was seen that both bacterial groups with the addition of only mHNTs had bacterial inhibition rates close to 0, which indicated that the bacterial growth in the mHNT group was similar to that with the addition of sterile water, denoting the non-antimicrobial nature of mHNTs. Aluminosilicate clay alone without antibacterial properties was found in previous studies,<sup>42,43</sup> which was consistent with our experimental results. However, the 0.5 wt % mHNT-stabilized cassia oil emulsion demonstrated a fast bacterial inhibition rate, reaching 97.7% inhibition of *S. aureus* and 97.4% inhibition of *E. coli* at 2 h, and maintained a stable rate of inhibition for 6 h. The faster bacterial inhibition rate proved that the loose and porous skeleton formed by the lesser emulsifier made the cassia oil have a faster release rate. Relatively, emulsions stabilized with 5 wt % rHNTs had reduced rates of bacterial inhibition. The high amount of rHNTs allowed the formation of a thickened shell layer of rHNTs even with a high water contact angle, reducing the release rate of cassia oil. 5 wt % mHNT-stabilized emulsions had the slowest growing bacterial inhibition rate, with over 90% bacterial inhibition after 4 h for both bacterial groups (95.7% for *S. aureus* and 96.1% for *E. coli*). The suitable wetting angle and the higher amount of mHNTs caused the emulsion to have a large amount of mHNTs wrapped around the outside of all the cassia oil droplets, triggering a slower release rate. The pure cassia oil group also had a fast-growing bacterial inhibition rate, but its long-term inhibition rate was slightly lower than that of the emulsion group. It could be explained that due to the hydrophobicity of cassia oil, it could not be uniformly dispersed in the medium, leading to insufficient antibacterial properties.

**3.7. Visualization of Antibactericidal Effects.** AO/EB dyes were used to directly observe the survival of bacteria after treatment with different materials (PBS, cassia oil–water mixture, rHNTs, and mHNT emulsions). AO dyes penetrate all bacteria to stain them green, while EB can only penetrate damaged dead bacteria to stain them red.<sup>44</sup> Thus, alive bacteria stained by the AO/EB dye appear green, while dead bacteria will appear red or orange-yellow (a mixture of green and red). As shown in Figure 7a,b most of the bacteria co-incubated with PBS showed substantial green fluorescence at all times, with only a few orange-red fluorescent spots which were caused by naturally apoptotic bacteria, indicating substantial bacterial survival. In contrast, the group of bacteria co-incubated with

cassia oil alone exhibited approximately 90% bacterial mortality at 1 h but decreased to 83.5% after 6 h. The phenomenon implied that cassia oil had a fast bactericidal efficiency against *S. aureus* but a weak long-lasting antibacterial ability. mHNT-based cassia oil emulsions exhibited slow and long-lasting antibacterial properties. These results indicate that the encapsulation of mHNTs enabled the hydrophobic cassia oil to be uniformly dispersed in the hydrophilic solution and slowly released.

#### 4. CONCLUSIONS

In summary, the present work showed the hydrophobic modification of HNTs by a ball-milling method. Morphology results showed the loss of lumen and size reduction of HNTs by ball milling. PTFE from the wall of the milling jar was anchored on the surfaces of the HNTs. The loading of PTFE imparted suitable wettability to the HNTs for use as emulsifiers in the preparation of Pickering emulsions. Pickering emulsions with hexadecane as the oil phase showed significantly enhanced ability of mHNTs to emulsify oil droplets, and increased milling time resulted in the formation of smaller droplets. Extended milling time led to the formation of more tightly packed emulsion droplets, implying the enhanced stability of the emulsion. The mHNTs could stabilize the emulsions by adsorption at the oil–water interface, and they supported the oil droplets by forming a three-dimensional network skeleton in the emulsion. mHNTs form a denser emulsion network due to their suitable wettability to enhance the stability of the emulsion. In addition, mHNTs as an emulsifier of cassia oil can effectively enhance its antibacterial properties. Bacterial growth kinetics experiments and live/dead bacterial viability assays further validated the improved antibacterial properties of mHNT emulsions and enabled the slow release of cassia oil due to the encapsulation of mHNTs. The present work demonstrated the great potential of mHNTs as emulsifiers for the preparation of Pickering emulsions, which show promising applications in food preservation.

#### ■ ASSOCIATED CONTENT

##### SI Supporting Information

The Supporting Information is available free of charge at <https://pubs.acs.org/doi/10.1021/acsanm.2c02410>.

TGA curves of PTFE, HNTs, and PTFE–HNTs and photographs of hexadecane emulsions stabilized by different concentrations of HNTs in different milling time after standing for 3 months (PDF)

#### ■ AUTHOR INFORMATION

##### Corresponding Author

Mingxian Liu – Department of Materials Science and Engineering, College of Chemistry and Materials Science, Jinan University, Guangzhou 511443, China; [orcid.org/0000-0002-5466-3024](https://orcid.org/0000-0002-5466-3024); Email: [liumx@jnu.edu.cn](mailto:liumx@jnu.edu.cn)

##### Authors

Cuiying Tan – Department of Materials Science and Engineering, College of Chemistry and Materials Science, Jinan University, Guangzhou 511443, China  
Puxiang Zhao – Department of Materials Science and Engineering, College of Chemistry and Materials Science, Jinan University, Guangzhou 511443, China

Youquan Zhou – Department of Materials Science and Engineering, College of Chemistry and Materials Science, Jinan University, Guangzhou 511443, China

Complete contact information is available at: <https://pubs.acs.org/10.1021/acsanm.2c02410>

#### Author Contributions

C.T. carried out the experiments, analyzed the data, and wrote the paper. P.Z. and Y.Z. performed the characterization of materials. M.L. reviewed and edited the manuscript. The final manuscript was read and approved by all authors.

#### Notes

The authors declare no competing financial interest.

#### ■ ACKNOWLEDGMENTS

This work was financially supported by the National Natural Science Foundation of China (52073121), the Natural Science Foundation of Guangdong Province (2019A1515011509), the Science and Technology Program of Guangzhou (202102010117), and the Fundamental Research Funds for the Central Universities (21622406).

#### ■ REFERENCES

- (1) Xue, X.; Dong, J.; He, H.; Wang, J.; Kong, D.; Wang, L. Emulsification and Stabilization of Diacylglycerol-In-Water Pickering Emulsions Stabilized by Ultrafine Grinding Oat Bran Insoluble Fiber-gelatinized Starch Hybrid Granules. *Food Hydrocolloids* **2021**, *112*, 106322.
- (2) Yan, X.; Ma, C.; Cui, F.; McClements, D. J.; Liu, X.; Liu, F. Protein-Stabilized Pickering Emulsions: Formation, Stability, Properties, and Applications in Foods. *Trends Food Sci. Technol.* **2020**, *103*, 293–303.
- (3) Yang, X.; Cai, J.; Chen, L.; Cao, X.; Liu, H.; Liu, M. Green Detergent Made of Halloysite Nanotubes. *Chem. Eng. J.* **2021**, *425*, 130623.
- (4) Wu, X.; Zhang, Q.; Wang, Z.; Xu, Y.; Tao, Q.; Wang, J.; Kong, X.; Sheng, K.; Wang, Y. Investigation of Construction and Characterization of Carboxymethyl Chitosan–Sodium Alginate Nanoparticles to Stabilize Pickering Emulsion Hydrogels for Curcumin Encapsulation and Accelerating Wound Healing. *Int. J. Biol. Macromol.* **2022**, *209*, 1837–1847.
- (5) Yu, T.; Swientoniewski, L. T.; Omarova, M.; Li, M.-C.; Negulescu, I. I.; Jiang, N.; Darvish, O. A.; Panchal, A.; Blake, D. A.; Wu, Q.; Lvov, Y. M.; John, V. T.; Zhang, D. Investigation of Amphiphilic Polypeptoid-Functionalized Halloysite Nanotubes as Emulsion Stabilizer for Oil Spill Remediation. *ACS Appl. Mater. Interfaces* **2019**, *11*, 27944–27953.
- (6) Wu, J.; Ma, G. H. Recent Studies of Pickering Emulsions: Particles Make the Difference. *Small* **2016**, *12*, 4633–4648.
- (7) Jiang, H.; Sheng, Y.; Ngai, T. Pickering Emulsions: Versatility of Colloidal Particles and Recent Applications. *Curr. Opin. Colloid Interface Sci.* **2020**, *49*, 1–15.
- (8) Lai, H.; Liu, Y.; Huang, G.; Chen, Y.; Song, Y.; Ma, Y.; Yue, P. Fabrication and Antibacterial Evaluation of Peppermint Oil-Loaded Composite Microcapsules by Chitosan-Decorated Silica Nanoparticles Stabilized Pickering Emulsion Templating. *Int. J. Biol. Macromol.* **2021**, *183*, 2314–2325.
- (9) Huang, Y.; Liu, H.; Liu, S.; Li, S. Cinnamon Cassia Oil Emulsions Stabilized by Chitin Nanofibrils: Physicochemical Properties and Antibacterial Activities. *J. Agric. Food Chem.* **2020**, *68*, 14620–14631.
- (10) Cui, F.; Zhao, S.; Guan, X.; McClements, D. J.; Liu, X.; Liu, F.; Ngai, T. Polysaccharide-Based Pickering Emulsions: Formation, Stabilization and Applications. *Food Hydrocolloids* **2021**, *119*, 106812.

- (11) Zhao, X.; Zhou, C.; Liu, M. Self-Assembled Structures of Halloysite Nanotubes: Towards the Development of High-Performance Biomedical Materials. *J. Mater. Chem. B* **2020**, *8*, 838–851.
- (12) Cheikh, D.; Majdoub, H.; Darder, M. An Overview of Clay-Polymer Nanocomposites Containing Bioactive Compounds for Food Packaging Applications. *Appl. Clay Sci.* **2022**, *216*, 106335.
- (13) Zhang, T.; Wang, W.; Zhao, Y.; Bai, H.; Wen, T.; Kang, S.; Song, G.; Song, S.; Komarneni, S. Removal of Heavy Metals and Dyes by Clay-Based Adsorbents: From Natural Clays to 1D and 2D Nanocomposites. *Chem. Eng. J.* **2021**, *420*, 127574.
- (14) Zeng, Q.; Yu, A.; Lu, G.; Paul, D. Clay-Based Polymer Nanocomposites: Research and Commercial Development. *J. Nanosci. Nanotechnol.* **2005**, *5*, 1574–1592.
- (15) Murugesan, S.; Scheibel, T. Copolymer/Clay Nanocomposites for Biomedical Applications. *Adv. Funct. Mater.* **2020**, *30*, 1908101.
- (16) Floody, M. C.; Theng, B. K. G.; Reyes, P.; Mora, M. L. Natural Nanoclays: Applications and Future Trends—A Chilean Perspective. *Clay Miner.* **2009**, *44*, 161–176.
- (17) Lu, T.; Gou, H.; Rao, H.; Zhao, G. Recent Progress in Nanoclay-Based Pickering Emulsion and Applications. *J. Environ. Chem. Eng.* **2021**, *9*, 105941.
- (18) Mo, S.; Pan, T.; Wu, F.; Zeng, M.; Huang, D.; Zhang, L.; Jia, L.; Chen, Y.; Cheng, Z. Facile one-step microwave-assisted modification of kaolinite and performance evaluation of pickering emulsion stabilization for oil recovery application. *J. Environ. Manage.* **2019**, *238*, 257–262.
- (19) Kpogbemabou, D.; Lecomte-Nana, G.; Aimable, A.; Bienia, M.; Niknam, V.; Carrion, C. Oil-In-Water Pickering Emulsions Stabilized by Phyllosilicates at High Solid Content. *Colloids Surf. A Physicochem. Eng. Asp.* **2014**, *463*, 85–92.
- (20) Panchal, A.; Rahman, N.; Konnova, S.; Fakhrullin, R.; Zhang, D.; Blake, D.; John, V.; Ivanov, E.; Lvov, Y. Clay Nanotube Liquid Marbles Enhanced with Inner Biofilm Formation for the Encapsulation and Storage of Bacteria at Room Temperature. *ACS Appl. Nano Mater.* **2020**, *3*, 1263–1271.
- (21) Stavitskaya, A.; Batasheva, S.; Vinokurov, V.; Fakhrullina, G.; Sangarov, V.; Lvov, Y.; Fakhrullin, R. Antimicrobial Applications of Clay Nanotube-Based Composites. *Nanomaterials* **2019**, *9*, 708.
- (22) Panchal, A.; Swientoniewski, L. T.; Omarova, M.; Yu, T.; Zhang, D.; Blake, D. A.; John, V.; Lvov, Y. M. Bacterial Proliferation on Clay Nanotube Pickering Emulsions for Oil Spill Bioremediation. *Colloids Surf., B* **2018**, *164*, 27–33.
- (23) Cavallaro, G.; Milioto, S.; Nigamatzyanova, L.; Akhatova, F.; Fakhrullin, R.; Lazzara, G. Pickering Emulsion Gels Based on Halloysite Nanotubes and Ionic Biopolymers: Properties and Cleaning Action on Marble Surface. *ACS Appl. Nano Mater.* **2019**, *2*, 3169–3176.
- (24) Lisuzzo, L.; Cavallaro, G.; Milioto, S.; Lazzara, G. Pickering Emulsions Stabilized by Halloysite Nanotubes: From General Aspects to Technological Applications. *Adv. Mater. Interfac.* **2022**, *9*, 2102346.
- (25) Heitz, J.; Švorčík, V.; Bačáková, L.; Ročková, K.; Ratajová, E.; Gumpenberger, T.; Bäuerle, D.; Dvořánková, B.; Kahr, H.; Graz, I.; Romanin, C. Cell Adhesion on Polytetrafluoroethylene Modified by UV-Irradiation in an Ammonia Atmosphere. *J. Biomed. Mater. Res., Part A* **2003**, *67A*, 130–137.
- (26) Xu, Z.; Gao, Y.; Meng, S.; Yang, B.; Pang, L.; Wang, C.; Liu, T. Mechanism and in Vivo Evaluation: Photodynamic Antibacterial Chemotherapy of Lysine-Porphyrin Conjugate. *Front. Microbiol.* **2016**, *7*, 242.
- (27) Abdullayev, E.; Joshi, A.; Wei, W.; Zhao, Y.; Lvov, Y. Enlargement of Halloysite Clay Nanotube Lumen by Selective Etching of Aluminum Oxide. *ACS Nano* **2012**, *6*, 7216–7226.
- (28) Cheng, H.; Frost, R. L.; Yang, J.; Liu, Q.; He, J. Infrared and Infrared Emission Spectroscopic Study of Typical Chinese Kaolinite and Halloysite. *Spectrochim. Acta, Part A* **2010**, *77*, 1014–1020.
- (29) Zhao, M.; Kuga, S.; Wu, M.; Huang, Y. Hydrophobic Nanocoating of Cellulose by Solventless Mechanical Milling. *Green Chem.* **2016**, *18*, 3006–3012.
- (30) Low, L. E.; Siva, S. P.; Ho, Y. K.; Chan, E. S.; Tey, B. T. Recent Advances of Characterization Techniques for the Formation, Physical Properties and Stability of Pickering Emulsion. *Adv. Colloid Interface Sci.* **2020**, *277*, 102117.
- (31) Qian, X.; Peng, G.; Ge, L.; Wu, D. Water-in-water Pickering Emulsions Stabilized by the Starch Nanocrystals with Various Surface Modifications. *J. Colloid Interface Sci.* **2022**, *607*, 1613–1624.
- (32) Cai, X.; Li, C.; Tang, Q.; Zhen, B.; Xie, X.; Zhu, W.; Zhou, C.; Wang, L. Assembling Kaolinite Nanotube at Water/Oil Interface for Enhancing Pickering Emulsion Stability. *Appl. Clay Sci.* **2019**, *172*, 115–122.
- (33) Lee, E.; Kim, D.; Kim, K. Distinctive Rheological Properties of Pickering Emulsions: from Their Origin to the Applications. *Korea Aust. Rheol. J.* **2022**, *34*, 91–103.
- (34) Yang, H.; Su, Z.; Meng, X.; Zhang, X.; Kennedy, J. F.; Liu, B. Fabrication and Characterization of Pickering Emulsion Stabilized by Soy Protein Isolate-Chitosan Nanoparticles. *Carbohydr. Polym.* **2020**, *247*, 116712.
- (35) Xiao, J.; Wang, X. a.; Perez Gonzalez, A. J. P.; Huang, Q. Kafirin Nanoparticles-Stabilized Pickering Emulsions: Microstructure and Rheological Behavior. *Food Hydrocolloids* **2016**, *54*, 30–39.
- (36) Jain, S.; Winuprasith, T.; Suphantharika, M. Design and Synthesis of Modified and Resistant Starch-Based Oil-In-Water Emulsions. *Food Hydrocolloids* **2019**, *89*, 153–162.
- (37) Yang, Y.; Fang, Z.; Chen, X.; Zhang, W.; Xie, Y.; Chen, Y.; Liu, Z.; Yuan, W. An Overview of Pickering Emulsions: Solid-Particle Materials, Classification, Morphology, and Applications. *Front. Pharmacol.* **2017**, *8*, 287.
- (38) Kulisic, T.; Radonic, A.; Katalinic, V.; Milos, M. Use of Different Methods for Testing Antioxidative Activity of Oregano Essential Oil. *Food Chem.* **2004**, *85*, 633–640.
- (39) Kaskatepe, B.; Kiymaci, M. E.; Suzuk, S.; Erdem, S. A.; Cesur, S.; Yildiz, S. Antibacterial Effects of Cinnamon Oil Against Carbapenem Resistant Nosocomial Acinetobacter Baumannii and Pseudomonas Aeruginosa Isolates. *Ind. Crops Prod.* **2016**, *81*, 191–194.
- (40) Sun, H.; Li, S.; Chen, S.; Wang, C.; Liu, D.; Li, X. Antibacterial and Antioxidant Activities of Sodium Starch Octenylsuccinate-Based Pickering Emulsion Films Incorporated with Cinnamon Essential Oil. *Int. J. Biol. Macromol.* **2020**, *159*, 696–703.
- (41) Ingram, G. I. C. Formation of Clear Zones with ‘Sensitive’ and ‘Resistant’ Staphylococcus aureus in Penicillin Plate Assays. *Microbiology* **1951**, *5*, 22–29.
- (42) Jana, S.; Kondakova, A. V.; Shevchenko, S. N.; Sheval, E. V.; Gonchar, K. A.; Timoshenko, V. Y.; Vasiliev, A. N. Halloysite Nanotubes with Immobilized Silver Nanoparticles for Anti-Bacterial Application. *Colloids Surf., B* **2017**, *151*, 249–254.
- (43) Zhang, Y.; Chen, Y.; Zhang, H.; Zhang, B.; Liu, J. Potent Antibacterial Activity of a Novel Silver Nanoparticle-Halloysite Nanotube Nanocomposite Powder. *J. Inorg. Biochem.* **2013**, *118*, 59–64.
- (44) Xiong, Z.; Zhang, X.; Zhang, S.; Lei, L.; Ma, W.; Li, D.; Wang, W.; Zhao, Q.; Xing, B. Bacterial Toxicity of Exfoliated Black Phosphorus Nanosheets. *Ecotoxicol. Environ. Saf.* **2018**, *161*, 507–514.

**Supporting Information**  
**Hydrophobic Halloysite Nanotubes via Ball Milling for Stable**  
**Pickering Emulsions: Implications for Food Preservation**

*Cuiying Tan, Puxiang Zhao, Youquan Zhou, Mingxian Liu*

Department of Materials Science and Engineering, College of Chemistry and Materials Science,

Jinan University, Guangzhou 511443, China

\*Corresponding author. Email: liumx@jnu.edu.cn

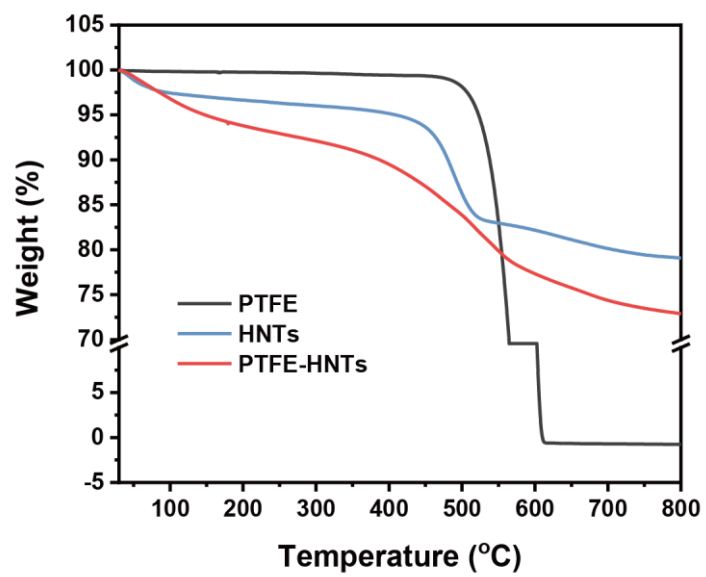


**Figure S1.** TGA curves of PTFE, HNTs and PTFE-HNTs.

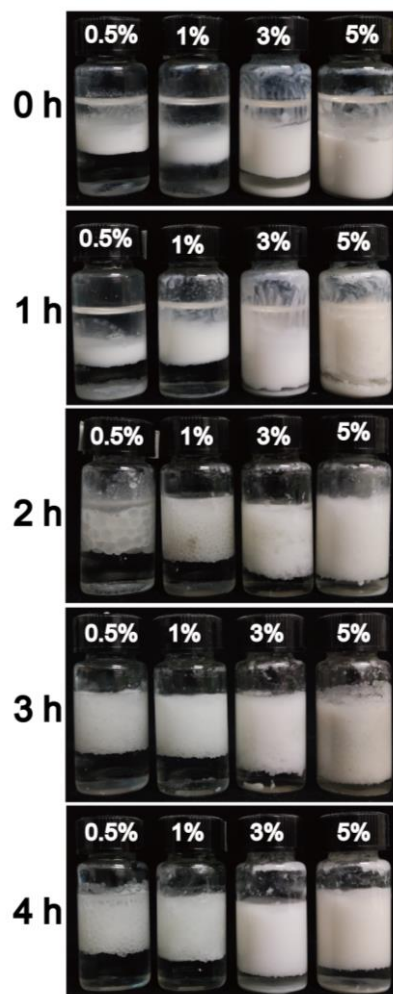


**Figure S2.** Photographs of hexadecane emulsions stabilized by different concentrations of HNTs in different milling time after standing for 3 months.